PHYSICS AND CHEMISTRY OF SOLID STATE
V. 25, No. 3 (2024) pp. 656-663
Section: Chemistry

DOI: 10.15330/pcss.25.3.656-663

Vasyl Stefanyk Precarpathian National University

ФІЗИКА І ХІМІЯ ТВЕРДОГО ТІЛА
Т. 25, № 3 (2024) С. 656-663
Хімічні науки

UDC: 544.344(043.5)

ISSN 1729-4428 (Print)
ISSN 2309-8589 (Online)

Andrii Selezen[1], Mykola Moroz[1], Yuri Kogut[2], Oleksandr Smitiukh[2], Vasyl Kordan[3], Lyudmyla Piskach[2]

Phase Equilibria in the Tl_2Te–$SiTe_2$ and Tl_2SiTe_3–Cd(Hg)Te Systems

[1]*National University of Water and Environmental Engineering, Rivne, Ukraine*
[2]*Lesya Ukrainka Volyn National University, Lutsk, Ukraine*
[3]*Ivan Franko National University of Lviv, Lviv, Ukraine, a.o.selezen@nuwm.edu.ua*

Component interaction in the Tl_2Te – $SiTe_2$ and Tl_2SiTe_3 – Cd(Hg)Te systems was investigated by X-ray diffraction (XRD), differential thermal analysis (DTA), and scanning electron microscopy with energy dispersive spectroscopy (SEM/EDS) methods. The formation of four new ternary tellurides $Tl_{18}SiTe_{11}$, Tl_4SiTe_4, Tl_2SiTe_3, and $Tl_2Si_2Te_5$, was found in the Tl_2Te – $SiTe_2$ system. The $Tl_{18}SiTe_{11}$ and Tl_2SiTe_3 compounds are formed congruently at 778 and 618 K, and Tl_4SiTe_4 and $Tl_2Si_2Te_5$ form incongruently at 546 and 584 K, respectively. Quaternary compounds $Tl_2CdSiTe_4$ and $Tl_2HgSiTe_4$ that form in the Tl_2SiTe_3 – Cd(Hg)Te systems crystallize in the tetragonal space group $I\text{–}42m$ and melt incongruently at 826 and 738 K, respectively. Each compound has a homogeneity region up to 5 mol.% from the Tl_2SiTe_3 side at 520 K.

Keywords: thallium tellurides, phase equilibria, solid solution, X-ray difraction, differential thermal analysis, scanning electron microscopy.

Received 16 May 2024; Accepted 10 September 2024.

Introduction

One of the current problems of chemistry is the search for new compounds which is accomplished by physico-chemical study of complex systems. The investigation of chalcogenide systems of the A^I – B^{II} – D^{IV} – X type (where A^I – Cu, Ag, Tl; B^{II} – Zn, Cd; D^{IV} – Si, Ge, Sn; X – S, Se, Te) expands the search for new semiconductor materials [1–6]. Quaternary phases of the $A^I_2B^{II}D^{IV}X_4$ type are often formed in such systems, individual representatives of which have already proven themselves in nonlinear optics and other areas of semiconductor technologies [7–17]. Recent studies of similar quaternary tellurides $Tl_2B^{II}D^{IV}Te_4$ (B^{II} – Cd, Hg, Mn; D^{IV} – Ge, Sn) confirm their thermoelectric properties [9, 17]. Additionally, these compounds crystallize in a non-centrosymmetric structure, thus they can exhibit nonlinear optical properties. Materials based on similar compounds with alkali metal elements that can be used in nonlinear optics and other areas were also reported [18–20]. Quaternary compounds of other compositions as well as ternary compounds are also formed in similar chalcogenide systems, for which fields of application were proposed taking into account their structure [21–24].

The components of the Tl_2Te – $SiTe_2$ system are semiconductor compounds. Tl_2Te crystallizes in the monoclinic space group (SG) $C2/c$, own structure type [25], and melts congruently at 698 K [26]. Silicon telluride $SiTe_2$ melts incongruently at 705 K and crystallizes in the trigonal SG $P\bar{3}m1$, CdI_2 structure type [27]. Bandgap energy for Tl_2Te is 0.64 eV [28], and 1.85 eV for $SiTe_2$ [29]. The existence of the Tl_2SiTe_3 compound in an unstable state is mentioned in [30], however, data on the method of its formation were not reported.

Binary semiconductor tellurides CdTe, HgTe that serve as components of the systems investigated in this work have narrow homogeneity regions. CdTe melts congruently at 1365 K [31] and crystallizes in the cubic SG $F\text{-}43m$ (sphalerite structure type), cell parameter a = 6.41 Å [32]. HgTe also melts congruently at 943 K

and crystallizes in the sphalerite structure with lattice period a = 6.37 Å [33]. CdTe is one of the important *n*-type semiconductors for the photovoltaic conversion of solar energy [34]. HgTe combined with CdTe ($Hg_xCd_{1-x}Te$) is the main material used for infrared detectors [35].The development and optimization of methods for synthesis of new multifunctional materials are based on data of the phase equilibria of the corresponding systems [36–38].

Ealier, we reported the synthesis and structure of the quaternary compounds $Tl_2Cd(Hg)SiTe_4$ [24] that crystallize in the tetragonal symmetry, SG *I*-42*m*, with the lattice parameters a = 8.4121(6), c = 7.0289(9) Å ($Tl_2CdSiTe_4$) and a = 8.3929(4), c = 7.0396(5) Å ($Tl_2HgSiTe_4$). Here, we present the results of an experimental study of polythermal sections Tl_2Te – $SiTe_2$ and Tl_2SiTe_3 – Cd(Hg)Te by differential thermal analysis (DTA) and X-ray diffraction (XRD) methods.

I. Experimental

Samples of the investigated systems were synthesized in an MP-60 muffle furnace from high-purity (at least 99.99 wt.%) elements Tl, Cd, Si, Te in evacuated to the residual pressure of 10^{-3} mm Hg and sealed quartz containers. The maximum synthesis temperature was 1000 K for the Tl_2Te–$SiTe_2$ system, all HgTe-containing alloys, and alloys in the range of 0–50 mol.% CdTe, and 1350 K for samples containing 50–100 mol.% CdTe. Homogenizing annealing was held for 250 hrs at 520 K, and the samples of the Tl_2Te – $SiTe_2$ system were annealed at 470 K. After annealing, the samples were quenched into room-temperature saline solution.

Powder X-ray diffraction spectra of the system samples were recorded at a DRON 4-13 diffractometer using CuKα radiation in the range of $10^o \le 2\Theta \le 80^o$, scan step 0.05º, 5 s exposure at each point. The boundaries of solid solutions were determined from X-ray diffraction data using the Rietveld method encoded in the CSD software package [39]. Differential thermal analysis utilized a computer-controlled set-up of a Thermodent-04 furnace and signal amplifier bloc with a combined Pt-Pt/Rh thermocouple and Al_2O_3 as a standard. DTA measurements were calibrated using reference substances In, Bi, Te, Sb, NaCl, Ag, Cu. Temperature measurement accuracy was ±5 K.

The composition of the $Tl_{18}SiTe_{11}$ compound was additionally investigated by scanning electron microscopy with energy dispersive spectroscopy (SEM/EDS) on the Tescan Vega 3 LMU microscope with an Oxford Instruments Aztec ONE X-ray microanalyzer and an X-Max^{N}20 detector, magnification x1000.

II. Results and discussion

2.1. The Tl_2Te–$SiTe_2$ system

The Tl_2Te–$SiTe_2$ system was investigated by the XRD and DTA methods to verify the existence of the Tl_2SiTe_3 compound. The existence of binary tellurides Tl_2Te and $SiTe_2$ was confirmed, and four new sets of reflections were found on the diffraction pattern that correspond to the compounds of the compositions $Tl_{18}SiTe_{11}$, Tl_4SiTe_4, Tl_2SiTe_3, $Tl_2Si_2Te_5$.

Diffraction patterns of compounds at the Tl_2Te – $SiTe_2$ section at 470 K are presented in Fig. 1. The formation of new ternary phases is observed at 10, 33.33, 50, and 66.67 mol.% $SiTe_2$.

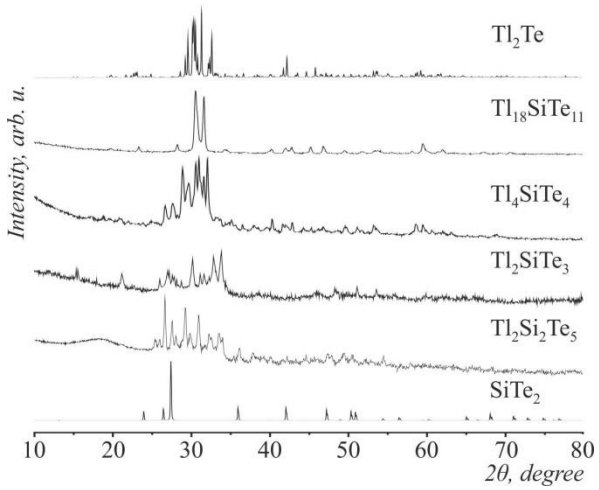

Fig. 1. Diffraction patterns of compounds of the Tl_2Te – $SiTe_2$ system at 470 K.

The investigated phase diagram (Fig. 2) shows that the Tl_2Te – $SiTe_2$ section is a quasi-binary system. DTA results are consistent with XRD data. The system liquidus is represented by seven curves of the primary crystallization of compounds Tl_2Te, $Tl_{18}SiTe_{11}$, Tl_4SiTe_4, LT-Tl_2SiTe_3, HT-Tl_2SiTe_3, $Tl_2Si_2Te_5$, and $SiTe_2$. Of the four new ternary tellurides, $Tl_{18}SiTe_{11}$ and Tl_2SiTe_3 melt congruently at 778 and 618 K, and Tl_4SiTe_4 and $Tl_2Si_2Te_5$ melt incongruently at 546 and 584 K, respectively.

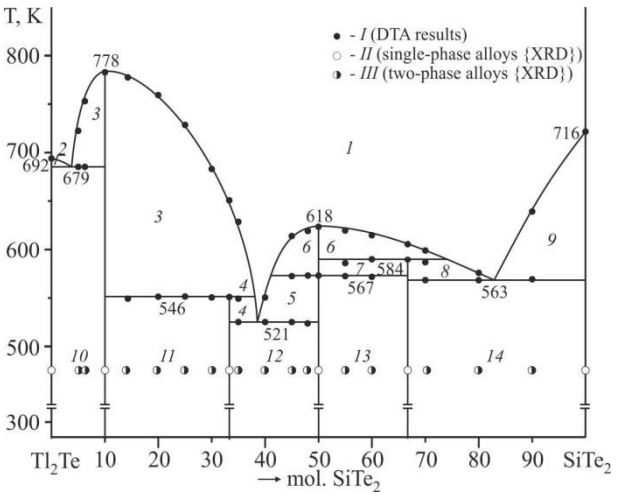

Fig. 2. Phase diagram of the Tl_2Te–$SiTe_2$ section:
1 – L; *2* – L + Tl_2Te; *3* – L + $Tl_{18}SiTe_{11}$; *4* – L + Tl_4SiTe_4; *5* – L + LT-Tl_2SiTe_3; *6* – L + HT-Tl_2SiTe_3; *7* – HT-Tl_2SiTe_3 + $Tl_2Si_2Te_5$; *8* – L + $Tl_2Si_2Te_5$; *9* – L + $SiTe_2$; *10* – Tl_2Te + $Tl_{18}SiTe_{11}$; *11* – $Tl_{18}SiTe_{11}$ + Tl_4SiTe_4; *12* – Tl_4SiTe_4 + LT-Tl_2SiTe_3; *13* – LT-Tl_2SiTe_3 + $Tl_2Si_2Te_5$; *14* – $Tl_2Si_2Te_5$ + $SiTe_2$.

Three invariant eutectic processes taking place in this system correspond to the reactions

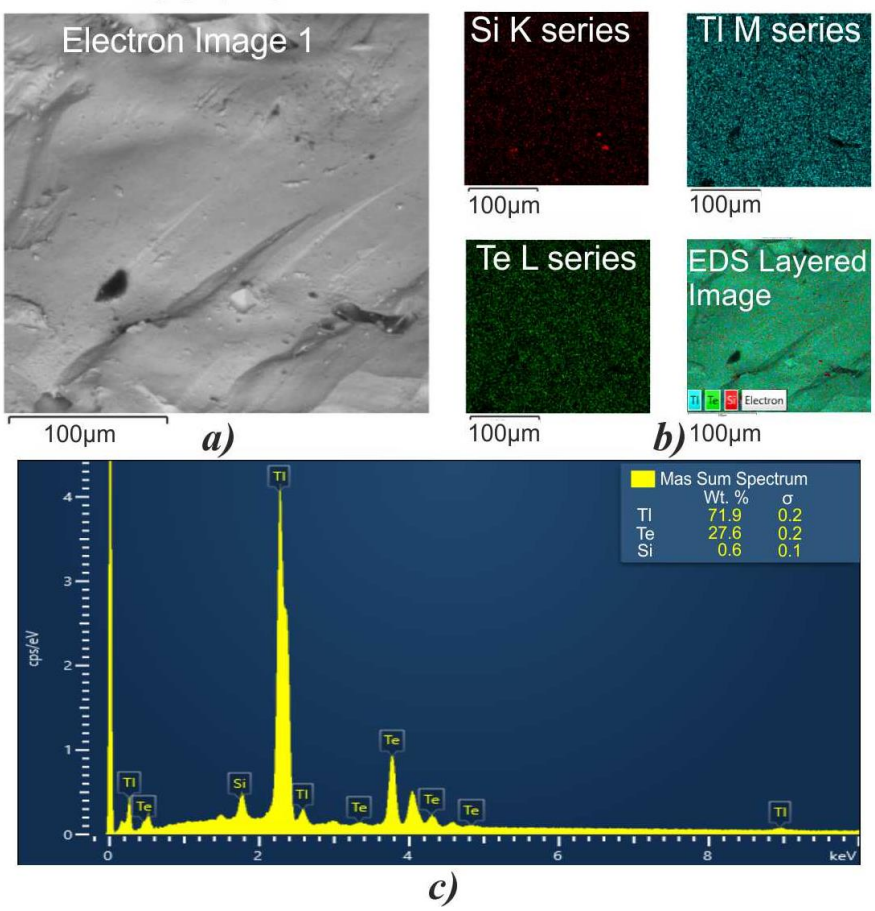

Fig. 3. SEM/EDS results for the $Tl_{18}SiTe_{11}$ compound: microphotograph of the sample surface (*a*), mapping results (*b*), elemental composition, wt.% (*c*).

$Le_1 \leftrightarrow Tl_2Te + Tl_{18}SiTe_{11}$ (4 mol.% $SiTe_2$, 679 K), $Le_2 \leftrightarrow Tl_4SiTe_4 + LT\text{-}Tl_2SiTe_3$ (38 mol.% $SiTe_2$, 521 K), $Le_3 \leftrightarrow Tl_2Si_2Te_5 + SiTe_2$ (83 mol.% $SiTe_2$, 563 K). Incongruent melting of Tl_4SiTe_4 is described by the peritectic reaction $L_{p1} + Tl_{18}SiTe_{11} \leftrightarrow Tl_4SiTe_4$ at 546 K. The $Tl_2Si_2Te_5$ compound forms in a peritectic reaction $L_{p2} + HT\text{-}Tl_2SiTe_3 \leftrightarrow Tl_2Si_2Te_5$ at 584 K. The horizontal at 567 K corresponds to the polymorphous transition of the equimolar compound Tl_2SiTe_3.

The sample with the input composition $Tl_{18}SiTe_{11}$ was additionally investigated by SEM/EDS to study the qualitative and quantitative composition. A micrograph of the sample surface is shown in Fig. 3 *a*. The results of qualitative elemental analysis are shows in Fig. 3 *b*. The results of the study of the elemental ratio of the sample are plotted in Fig. 3 *c*. The averaged result of the research is the composition $Tl_{18}Si_{1.09}Te_{11.06}$ which agrees well with the ratio of Tl:Si:Te atoms of 18:1:11.

2.2. The Tl_2SiTe_3–CdTe system

Phase equilibria in the Tl_2SiTe_3 – CdTe system were investigated on 17 alloys. Typical XRD patterns of alloys are shown in Fig. 4. The existence of the quaternary phase $Tl_2CdSiTe_4$ was confirmed. The phase has a homogeneity range of 45–50 mol.% CdTe that can be expressed as $Tl_{2+x}Cd_{1-1.5x}Si_{1+x/2}Te_4$ where x=0-0.1. The lattice periods at the annealing temperature 520 K satisfy Vegard's rule and vary linearly in rande a = 8.4121-8.4352 Å, and c = 7.0289-7.0026 Å. The inclusion of silicon atoms with a smaller radius and cadmium atoms with a larger radius is stoichiometric and leads to an increase in cell parameters. The presence of heavy atoms of elements is important to improve some properties of materials, for example thermoelectric. As result of the substitution in this material, the metallic component is increased, which will lead to decrease of band gap. The results presented in [24] refer to the extreme point corresponding to the $Tl_2CdSiTe_4$ composition, which corresponds to the ratio of the initial components 2Tl:1Cd:1Si:4Te. Variation of the crystal lattice parameters in the solid solution range of the quaternary compound at 520 K is plotted in Fig. 5. A graphical representation of the change in unit cell parameters within a solid solution based on a quaternary compound $Tl_2CdSiTe_4$ at 520 K is shown in Fig. 5. Solid solubility based on CdTe is less than 3 mol.%.

Phase diagram of the Tl_2SiTe_3 – CdTe system is presented in Fig. 6. The system is a quasi-binary section in the quasi-ternary system Tl_2Te – CdTe – $SiTe_2$. The liquidus is represented by four curves of the primary crystallization of high-temperature modification of HT-Tl_2SiTe_3, α- and α'-solid solutions of HT and LT modifications of $Tl_2CdSiTe_4$, and β-solid solution of CdTe. According to DTA results, the quaternary phase melts incongruently in the peritectic process $Lp + \beta\text{-CdTe} \leftrightarrow \alpha'\text{-}Tl_2CdSiTe_4$ at 826 K. The composition of the peritectic point was determined by extrapolation of three lines to their intersection at 32 mol.% CdTe. Polymorphous transition of the quaternary phase occurs at 613 K. The eutectic process at 602 K corresponds to the equilibrium $Le \leftrightarrow HT\text{-}Tl_2SiTe_3 + \alpha\text{-}Tl_2CdSiTe_4$; the

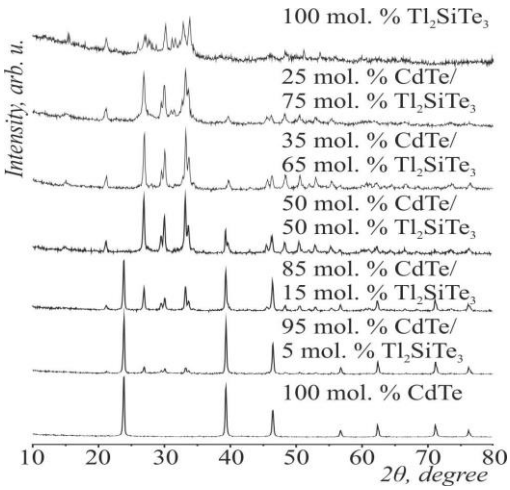

Fig. 4. Diffraction patterns of alloys of the Tl_2SiTe_3–CdTe system.

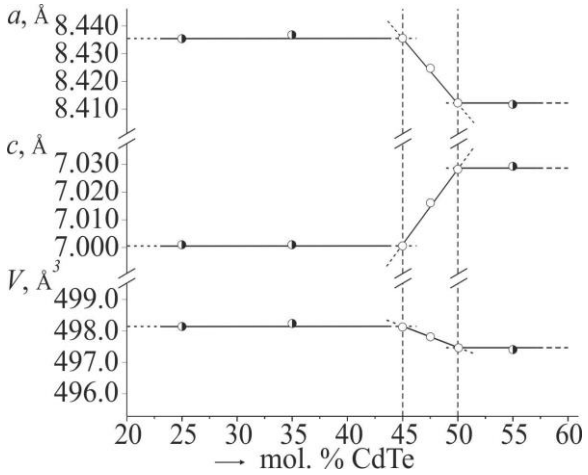

Fig. 5. Variation of the lattice parameters of alloys of the Tl_2SiTe_3–CdTe system at 520 K.

eutectic point is at 10 mol.% CdTe. The horizontal at 564 K corresponds to the polymorphous transition of Tl_2SiTe_3.

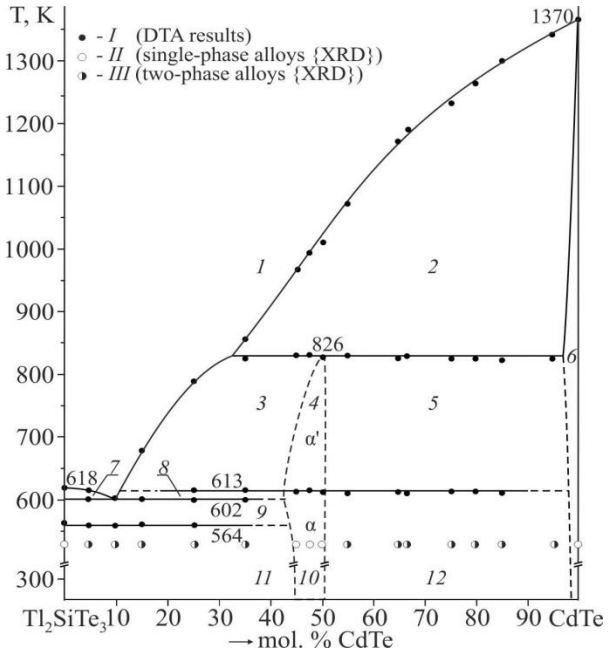

Fig. 6. Phase diagram of the Tl_2SiTe – CdTe section:
1 – L; *2* – L + β-CdTe; *3* – L + α'-$Tl_2CdSiTe_4$;
4 – α'-$Tl_2CdSiTe_4$; *5* – α'-$Tl_2CdSiTe_4$ + β-CdTe;
6 – β-CdTe; *7* – L + HT-Tl_2SiTe_3; *8* – L + α-$Tl_2CdSiTe_4$;
9 – HT-Tl_2SiTe_3 + α-$Tl_2CdSiTe_4$; *10* – α-$Tl_2CdSiTe_4$;
11 – LT-Tl_2SiTe_3 + α-$Tl_2CdSiTe_4$;
12 – α-$Tl_2CdSiTe_4$ + β-CdTe.

DTA curve for the equimolar sample of the Tl_2SiTe_3 – CdTe system is plotted in Fig. 7. It features three endothermic effects at 613, 826, and 988 K, which correspond to the α ↔ α' phase transition of the $Tl_2CdSiTe_4$ compound, the peritectic melting of $Tl_2CdSiTe_4$, and the liquidus temperature, respectively. Three exothermic effects are also present corresponding to these processes during cooling, demonstrating substantial supercooling.

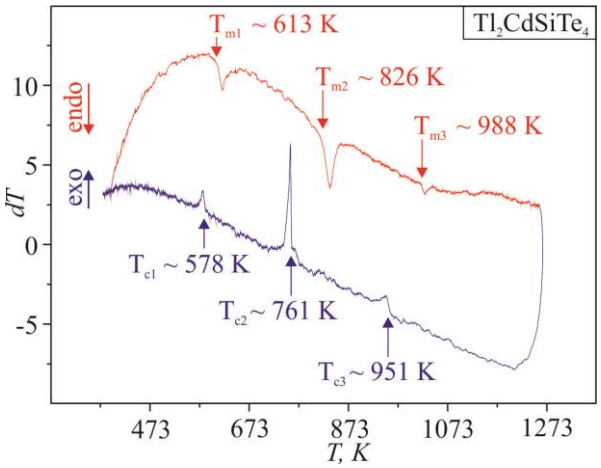

Fig. 7. DTA curve for the sample of $Tl_2CdSiTe_4$ composition.

2.3. The Tl_2SiTe_3 – HgTe system

The Tl_2SiTe_3 – HgTe system was investigated by XRD and DTA methods. Diffraction patterns of typical samples of the system are presented in Fig. 8. As in the cadmium-containing system, the existence of the corresponding quaternary compound $Tl_2HgSiTe_4$ was confirmed that crystallizes in the tetragonal structure, SG *I*–42*m* [24]. Similarly, the mercury-containing quaternary compound has a homogeneity range 45–50 mol.% HgTe ($Tl_{2+x}Hg_{1-1.5x}Si_{1+x/2}Te_4$, x = 0-0.1). The change in the parameters of the unit cell of the solid solution is linear, corresponding to the Wegard rule, and is at the homogenization annealing temperature in ranges: a = 8.3929(4)-8.3972(2) Å, and c = 7.0396(5)-7.0122(4) Å. The change of the lattice parameters within the solid solution range of $Tl_2HgSiTe_4$ at 520 K is plotted in Fig. 9.

The system is a quasi-binary section, its liquidus is represented by three curves of the primary crystallization of HT-Tl_2SiTe_3 and α and β solid solutions of $Tl_2CdSiTe_4$ and HgTe, respectively (Fig. 10). The coordinates of the peritectic process Lp + β-HgTe ↔ α-$Tl_2HgSiTe_4$ are 42 mol.% HgTe at 738 K. The system undergoes an invariant eutectic process corresponding to the equilibrium Le ↔ HT-Tl_2SiTe_3 + α-$Tl_2HgSiTe_4$, with the eutectic point at 12 mol.% HgTe, 582 K).

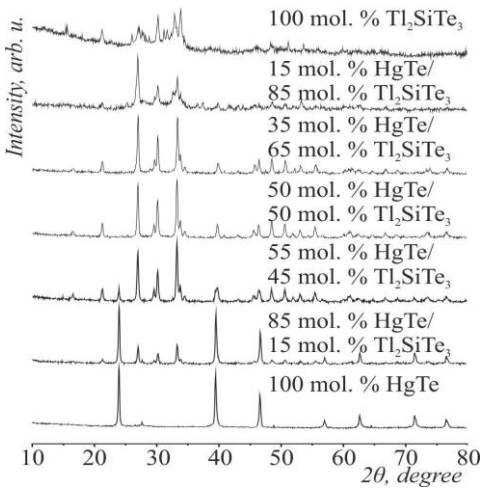

Fig. 8. Diffraction patterns of samples of the Tl_2SiTe – HgTe system at 520 K.

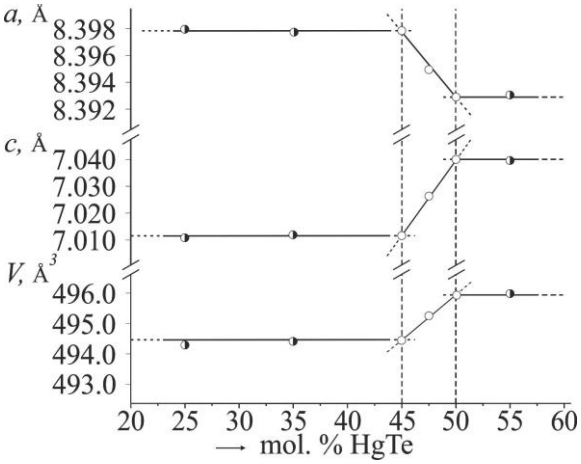

Fig. 9. Change of the lattice parameters of samples of the Tl_2SiTe_3 – HgTe system at 520 K.

The samples up to 25 mol.% HgTe feature an effect at 565 K that corresponds to the polymorphous transition of the ternary phase Tl_2SiTe_3. The thermogram of the sample of the 95 mol.% HgTe composition features an effect corresponding to the peritectic process, therefore solid solubility based on HgTe is less than 3 mol.%.

The incongruent melting of the $Tl_2HgSiTe_4$ compound is illustrated by the DTA curve (Fig. 11) for this sample (50 mol.% Tl_2SiTe_3/50 mol.% HgTe). This is characterized by the broad endothermic effect upon heating which can be divided into two, at 738 and 765 K. We can assert this as the two exothermic effects upon cooling are clearly separated. The first process at 738 K corresponds to the peritectic formation of the $Tl_2HgSiTe_4$ compound, the second is the liquidus temperature.

Conclusions

Polythermal sections Tl_2Te – $SiTe_2$ and Tl_2SiTe_3 – Hg(Cd)Te were studied using XRD and DTA methods. The formation of four new ternary tellurides $Tl_{18}SiTe_{11}$ (10 mol.% $SiTe_2$), Tl_4SiTe_4 (33.3 mol.% $SiTe_2$), Tl_2SiTe_3 (50 mol.% $SiTe_2$), $Tl_2Si_2Te_5$ (66.7 mol.% $SiTe_2$) was established in the Tl_2Te – $SiTe_2$ system. The qualitative and quantitative composition of the ternary compound $Tl_{18}SiTe_{11}$ was confirmed by SEM/EDS. Phase diagrams for the three sections were constructed. The compounds $Tl_2HgSiTe_4$ and $Tl_2CdSiTe_4$ each has a homogeneity region of up to 5 mol.% at 520 K. New semiconductor ternary and quaternary compounds found in these systems may find application as nonlinear optical materials.

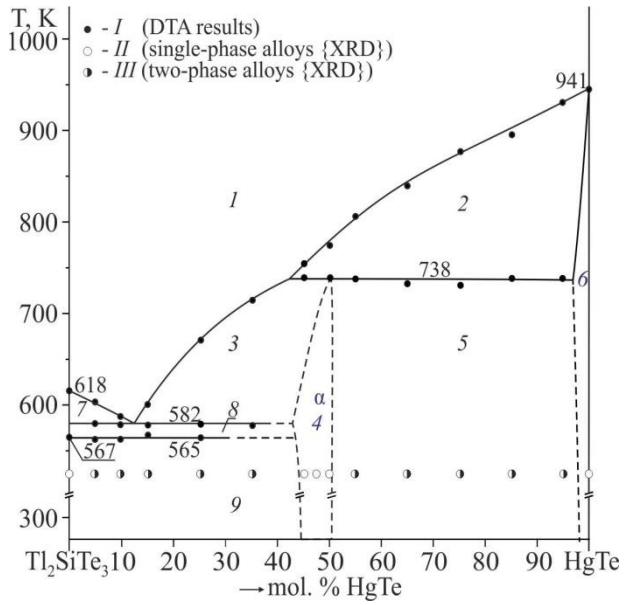

Fig. 10. Phase diagram of the Tl_2SiTe_3 – HgTe section: *1* – L; *2* – L + β-HgTe; *3* – L + α-$Tl_2HgSiTe_4$; *4* – α-$Tl_2HgSiTe_4$; *5* – α-$Tl_2HgSiTe_4$ + β-HgTe; *6* – β-HgTe; *7* – L + HT-Tl_2SiTe_3; *8* – HT-Tl_2SiTe_3 + α-$Tl_2HgSiTe_4$; *9* – HT-Tl_2SiTe_3 + α-$Tl_2HgSiTe_4$.

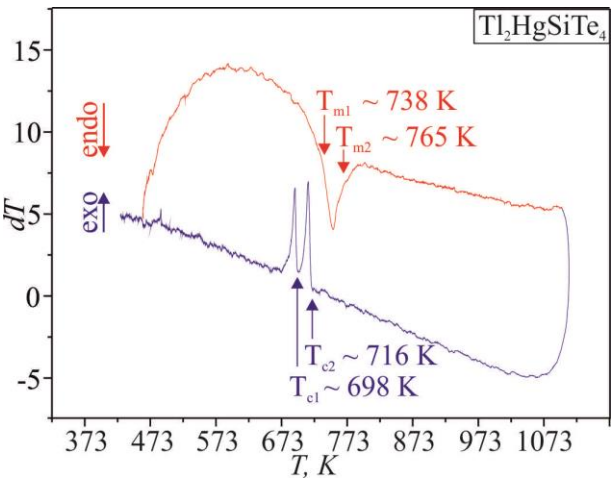

Fig. 11. DTA curve for the sample of the $Tl_2HgSiTe_4$ composition.

Selezen Andrii – Ph. D. in Chemistry, Senior Instructor of the Department of Chemistry and Physics of National University of Water and Environmental Engineering;
Moroz Mykola – D. Sc. in Chemistry, Professor, Head of the Department of Chemistry and Physics of National University of Water and Environmental Engineering;
Kogut Yuri – Ph. D. in Chemistry, Senior Instructor of the Department of Chemistry and Technology of Lesya Ukrainka Volyn National University;
Smitiukh Oleksandr – Ph. D. in Chemistry, Senior Instructor of the Department of Chemistry and Technology of Lesya Ukrainka Volyn National University;
Kordan Vasyl – Ph. D. in Chemistry, Research Fellow of the Department of Inorganic Chemistry of Ivan Franko National University of Lviv;
Piskach Lyudmyla – Ph. D. in Chemistry, Professor, Department of Inorganic and Physical Chemistry of Lesya Ukrainka Volyn National University.

[1] G. Eulenberger, *Darstellung und Kristallstruktur des Dithallium (I) blei (II) tetra- thiogermanats (IV) Tl_2PbGeS_4*, Z. Naturforsch. B. 35, 335 (1980); https://doi.org/10.1515/znb-1980-0315.
[2] O.V. Parasyuk, L.D. Gulay, L.V. Piskach, O.P. Gagalovska, *The $Ag_2S–HgS–GeS_2$ system at 670 K and the crystal structure of the Ag_2HgGeS_4 compound*, J. Alloys Compd., 336, 213(2002); https://doi.org/10.1016/S0925-8388(01)01904-1.
[3] I.D. Olekseyuk, L.V. Piskach, O.Ye. Zhbankov, O.V. Parasyuk, Yu.M. Kogut, *Phase diagrams of the quasi-binary systems $Cu_2S–SiS_2$ and $Cu_2SiS_3–PbS$ and the crystal structure of the new quaternary compound Cu_2PbSiS_4*, J. Alloys Compd., 399, 149 (2005); https://doi.org/10.1016/j.jallcom.2005.03.086.
[4] L.P. Marushko, L.V. Piskach, O.V. Parasyuk, I.D. Olekseyuk, S.V. Volkov, V.I. Pekhnyo, *The reciprocal system $Cu_2GeS_3+3CdSe⇔Cu_2GeSe_3+3CdS$*, J. Alloys Compd., 473, 94 (2009); https://doi.org/10.1016/j.jallcom.2008.05.073.
[5] C.D. Brunetta, W.C. Minsterman, C.H. Lake, J.A. Aitken, *Cation ordering and physicochemical characterization of the quaternary diamond-like semiconductor Ag_2CdGeS_4*, J. Solid State Chem., 187, 177 (2012); https://doi.org/10.1016/j.jssc.2011.12.032.
[6] M.Yu. Mozolyuk, L.V. Piskach, A.O. Fedorchuk, I.D. Olekseyuk, O.V. Parasyuk, *Phase equilibria in the $Tl_2S–PbS–GeS_2$ system and crystal structure of $Tl_{0.5}Pb_{1.75}GeS_4$*, Chem. Met. Alloys, 5, 37 (2012); http://dx.doi.org/10.30970/cma5.0205.
[7] I. Tsuji, Y. Shimodaira, H. Kato, H. Kobayashi, A. Kudo, *Novel Stannite-type Complex Sulfide Photocatalysts A^I_2 -Zn-A^{IV}-S_4 (A^I = Cu and Ag; A^{IV} = Sn and Ge) for Hydrogen Evolution under Visible-Light Irradiation*, Chem. Mater., 22, 1402 (2010); https://doi.org/10.1021/cm9022024.
[8] C. Wang, S. Chen, J.-H. Yang, L. Lang, H.-J. Xiang, X.-G. Gong, A. Walsh, S.-H. Wei, *Design of $I_2–II–IV–VI_4$ Semiconductors through Element Substitution: The Thermodynamic Stability Limit and Chemical Trend*, Chem. Mater., 26, 3411 (2014); https://doi.org/10.1021/cm500598x.
[9] M.A. McGuire, T.J. Scheidemantel, J.V. Badding, F.J. DiSalvo, *Tl_2AXTe_4 (A = Cd, Hg, Mn; X = Ge, Sn): Crystal Structure, Electronic Structure, and Thermoelectric Properties*, Chem. Mater., 17, 6186 (2005); https://doi.org/10.1021/cm0518067.
[10] C. Rincón, M. Quintero, E. Moreno, Ch. Power, E. Quintero, J.A. Henao, M.A. Macías, *Raman spectrum of $Cu_2CdSnSe_4$ stannite structure semiconductor compound*, Superlattices Microstruct., 88, 99 (2015); https://doi.org/10.1016/j.spmi.2015.08.032.
[11] M.Ya. Valakh, V.O. Yukhymchuk, I.S. Babichuk, Ye.O. Havryliuk, O.V. Parasyuk, L.V. Piskach, A.P. Litvinchuk, *Vibrational spectroscopy of orthorhombic Cu_2ZnSiS_4 single crystal: Low-temperature polarized Raman scattering and first principle calculations*, Vib. Spectrosc., 89, 81 (2017); https://doi.org/10.1016/j.vibspec.2017.01.005.
[12] H. Guo, C. Ma, K. Zhang, X. Jia, Y. Li, N. Yuan, J. Ding, *The fabrication of Cd-free Cu_2ZnSnS_4-Ag_2ZnSnS_4 heterojunction photovoltaic devices*, Sol. Energy Mater. Sol. Cells, 178, 146 (2018); https://doi.org/10.1016/j.solmat.2018.01.022.
[13] E. Hajdeu-Chicarosh, *Variable-Range Hopping Conduction in the Kesterite and Wurtzstannite Cu_2ZnGeS_4 Single Crystals*, Surf. Eng. Appl. Electrochem., 54, 279 (2018); https://doi.org/10.3103/S1068375518030055.
[14] M. Moroz, F. Tesfaye, P. Demchenko, M. Prokhorenko, D. Lindberg, O. Reshetnyak, L. Hupa, *Thermal Stability and Thermodynamics of the Ag_2ZnGeS_4 Compound*, Mater. Process. Fundam., 215 (2019); https://doi.org/10.1007/978-3-030-05728-2_20.
[15] Y. Jiang, B. Yao, J. Jia, Z. Ding, R. Deng, D. Liu, Y. Sui, H. Wang, Y. Li, *Structural, electrical, and optical properties of $Ag_2ZnSnSe_4$ for photodetection application*, J. Appl. Phys., 125, 025703 (2019); https://doi.org/10.1063/1.5055895.
[16] H.M. Mohammedi, F. Chiker, H. Khachai, N. Benosman, R. Khenata, R. Ahmed, S.B. Omran, A. Bouhemadou, X. Wang, *Structural, optoelectronic, optical coating and thermoelectric properties of the chalcogenides type Kesterite Ag_2CdSnX_4 (with X=S, Se): A computational insight*, Mater. Sci. Semicond. Process., 134, 106031 (2021); https://doi.org/10.1016/j.mssp.2021.106031.
[17] S. Hasan, S. San, K. Baral, N. Li, P. Rulis, W.-Y. Ching, *First-Principles Calculations of Thermoelectric Transport Properties of Quaternary and Ternary Bulk Chalcogenide Crystals*, Materials. 15, 2843 (2022); https://doi.org/10.3390/ma15082843.

[18] J.-H. Zhang, D.J. Clark, A. Weiland, S.S. Stoyko, Y.S. Kim, J.I. Jang, J.A. Aitken, *$Li_2CdGeSe_4$ and $Li_2CdSnSe_4$: biaxial nonlinear optical materials with strong infrared second-order responses and laser-induced damage thresholds influenced by photoluminescence*, Inorg. Chem. Front., 4, 1472 (2017); https://doi.org/10.1039/C7QI00004A.

[19] J.A. Brant, D.J. Clark, Y.S. Kim, J.I. Jang, J.-H. Zhang, J.A. Aitken, Li_2CdGeS_4, *A Diamond-Like Semiconductor with Strong Second-Order Optical Nonlinearity in the Infrared and Exceptional Laser Damage Threshold*, Chem. Mater., 26, 3045 (2014); https://doi.org/10.1021/cm501029s.

[20] S. Azam, S.A. Khan, S. Goumri-Said, *Modified Becke–Johnson (mBJ) exchange potential investigations of the optoelectronic structure of the quaternary diamond-like semiconductors Li_2CdGeS_4 and Li_2CdSnS_4*, Mater. Sci. Semicond. Process. 39, 606 (2015); https://doi.org/10.1016/j.mssp.2015.05.068.

[21] O.V. Zamuruieva, M.V. Khvyshchu, O.V. Parasyuk, G.L. Myronchuk, *Electric and photoelectric properties of solid solutions $Ag_2In_2Si(Ge)Se_6$*, Phys. Chem. Solid State. 17, 202 (2016); https://doi.org/10.15330/pcss.17.2.202-206.

[22] O.V. Tsisar, L.V. Piskach, O.V. Parasyuk, O.V. Zamurujeva, G.L. Myronchuk, M. Piasecki, *$Tl_2S–In_2S_3–GeS_2$ Glass System as Novel Promising Materials for Photonics*, Phys. Chem. Solid State. 20, 416 (2019); https://doi.org/10.15330/pcss.20.4.416-422.

[23] G.L. Myronchuk, O.V. Zamurujeva, I.V. Kityk, *IR Photoinduced Piezoelectric Effects in Multi-Component Chalcogenides $Ag_2In(Ga)_2Si(Ge)S(Se)_6$*, Phys. Chem. Solid State, 20, 401 (2019); https://doi.org/10.15330/pcss.20.4.401-405.

[24] A.O. Selezen, I.D. Olekseyuk, G.L. Myronchuk, O.V. Smitiukh, L.V. Piskach, *Synthesis and structure of the new semiconductor compounds $Tl_2B^{II}D^{IV}X_4$ (B^{II}–Cd, Hg; D^{IV}– Si, Ge; X–Se, Te) and isothermal sections of the $Tl_2Se–CdSe$-$Ge(Sn)Se_2$ systems at 570 K*, J. Solid State Chem., 289, 121422 (2020); https://doi.org/10.1016/j.jssc.2020.121422.

[25] R. Černý, J.-M. Joubert, Y. Filinchuk, Y. Feutelais, *Tl_2Te and its relationship with Tl_5Te_3*, Acta Crystallogr. C, 58, i63 (2002); https://doi.org/10.1107/S0108270102005085.

[26] F. Römermann, Y. Feutelais, S.G. Fries, R. Blachnik, *Phase diagram experimental investigation and thermodynamic assessment of the thallium–selenium system*, Intermetallics, 8, 53 (2000); https://doi.org/10.1016/S0966-9795(99)00068-0.

[27] R. Mishra, P.K. Mishra, S. Phapale, P.D. Babu, P.U. Sastry, G. Ravikumar, A.K. Yadav, *Evidences of the existence of $SiTe_2$ crystalline phase and a proposed new Si–Te phase diagram*, J. Solid State Chem., 237, 234 (2016); https://doi.org/10.1016/j.jssc.2016.02.021.

[28] *Materials Data on Tl_2Te by Materials Project* (2020); https://doi.org/10.17188/1277004.

[29] J.W. Rau, C.R. Kannewurf, *Intrinsic absorption and photoconductivity in single crystal $SiTe_2$*, J. Phys. Chem. Solids, 27, 1097 (1966); https://doi.org/10.1016/0022-3697(66)90085-0.

[30] A. Assoud, N. Soheilnia, H. Kleinke, *Crystal structure, electronic structure and physical properties of the new low-valent thallium silicon telluride $Tl_6Si_2Te_6$ in comparison to $Tl_6Ge_2Te_6$*, J. Solid State Chem., 179, 2707 (2006); https://doi.org/10.1016/j.jssc.2006.05.029.

[31] P. Seller, S. Bell, R.J. Cernik, C. Christodoulou, C.K. Egan, J.A. Gaskin, S. Jacques, S. Pani, B.D. Ramsey, C. Reid, P.J. Sellin, J.W. Scuffham, R.D. Speller, M.D. Wilson, M.C. Veale, *Pixellated Cd(Zn)Te high-energy X-ray instrument*, J. Instrum., 6, C12009 (2011); https://doi.org/10.1088/1748-0221/6/12/C12009.

[32] T.R. Shojaei, M.A.M. Salleh, K. Sijam, R.A. Rahim, A. Mohsenifar, R. Safarnejad, M. Tabatabaei, *Fluorometric immunoassay for detecting the plant virus Citrus tristeza using carbon nanoparticles acting as quenchers and antibodies labeled with CdTe quantum dots*, Microchim. Acta, 183, 2277 (2016); https://doi.org/10.1007/s00604-016-1867-7.

[33] W.H. Zachariasen, *Die Kristallstruktur der Telluride von Zink, Cadmium und Quecksilber*, Norsk Geologisk Tidsskrift, 8, 302 (1926).

[34] I.Y. Borg, D.K. Smith, *X-ray diffraction studies on CdTe at high pressure*, J. Phys. Chem. Solids, 28, 49 (1967); https://doi.org/10.1016/0022-3697(67)90196-5.

[35] I.M. Baker, *Properties of Narrow Gap Cadmium-Based Compounds*, EMIS Datareviews Series, 10, 323 (1994).

[36] M. Moroz, F. Tesfaye, P. Demchenko, M. Prokhorenko, Y. Kogut, O. Pereviznyk, S. Prokhorenko, O. Reshetnyak, *Solid-state electrochemical synthesis and thermodynamic properties of selected compounds in the Ag–Fe–Pb–Se system*, Solid State Sci., 107, 106344 (2020); https://doi.org/10.1016/j.solidstatesciences.2020.106344.

[37] G.S. Hasanova, A.I. Aghazade, D.M. Babanly, S.Z. Imamaliyeva, Y.A. Yusibov, M.B. Babanly, *Experimental study of the phase relations and thermodynamic properties of Bi-Se system*, J. Therm. Anal. Calorim., 147, 6403 (2022); https://doi.org/10.1007/s10973-021-10975-0.

[38] M.B. Babanly, Y. A.Yusibov, S.Z. Imamaliyeva, D. M.Babanly, I. J.Alverdiyev, *Phase Diagrams in the Development of the Argyrodite Family Compounds and Solid Solutions Based on Them*, J. Phase Equilib. Diffus., (2024); https://doi.org/10.1007/s11669-024-01088-w.

[39] L. Akselrud, Y. Grin, *WinCSD8: software package for crystallographic calculations (Version 4)*, J. Appl. Crystallogr., 47, 803 (2014); https://doi.org/10.1107/S1600576714001058.

Андрій Селезень[1], Микола Мороз[1], Юрій Когут[2], Олександр Смітюх[2], Василь Кордан[3], Людмила Піскач[2]

Фазові рівноваги в системах $Tl_2Te–SiTe_2$ та $Tl_2SiTe_3–Hg(Cd)Te$

[1]*Національний університет водного господарства та природокористування, Рівне, Україна*
[2]*Волинський національний університет імені Лесі Українки, Луцьк, Україна*
[3]*Львівський національний університет імені Івана Франка, Львів, Україна, a.o.selezen@nuwm.edu.ua*

Методами рентгенофазового (РФА), диференційно-термічного (ДТА) та спектроемісійного (СЕМ/ЕДС) аналізів проведено експериментальне дослідження фізико-хімічної взаємодії компонентів у халькогенідних системах Tl_2Te – $SiTe_2$ та Tl_2SiTe_3 – Cd(Hg)Te. У квазібінарній системі Tl_2Te – $SiTe_2$ при співвідношенні компонентів як 10, 33.33, 50 та 66.67 мол.% $SiTe_2$ спостерігається утворення чотирьох нових тернарних телуридів, які відповідають молекулярним складам: $Tl_{18}SiTe_{11}$, Tl_4SiTe_4, Tl_2SiTe_3 та $Tl_2Si_2Te_5$ відповідно. Сполуки $Tl_{18}SiTe_{11}$ та Tl_2SiTe_3 характеризуються конгруентним типом утворення при 778 та 618 К. Телуриди Tl_4SiTe_4 та $Tl_2Si_2Te_5$ плавляться інконгруентно при 546 та 584 К відповідно. Методом скануючої електронної мікроскопії у комплексі з енергодисперсною спектроскопією підтверджено якісний та кількісний склад нової тернарної сполуки $Tl_{18}SiTe_{11}$, що становить $Tl_{18}Si_{1.09}Te_{11.06}$. У системах Tl_2SiTe_3 – Cd(Hg)Te інконгруентно утворюються тетрарні сполуки $Tl_2CdSiTe_4$ та $Tl_2HgSiTe_4$ при 826 та 738 К відповідно. Сполуки кристалізуються в нецентросиметричній структурі тетрагональної сингонії ПГ *I*-42*m* та мають область гомогенності до 5 мол.% зі сторони Tl_2SiTe_3 при 520 К. В інтервалі існування фази складу $Tl_{2+x}Cd_{1-1.5x}Si_{1+x/2}Te_4$, де x = 0.1 періоди гратки при температурі гомогенізуючого відпалу змінюються у діапазоні: a = 8.4121 - 8.4352 Å, а період c = 7.0289 - 7.0026 Å. Встановлено існування твердого розчину на основі тетрарної фази $Tl_2HgSiTe_4$, протяжність якого змінюється в діапазоні концентрацій $Tl_{2+x}Hg_{1–1.5x}Si_{1+x/2}Te_4$, де x = 0.1, а періоди гратки при цьому змінюються в межах: a = 8.3929 - 8.3972 Å та c = 7.0396 - 7.0122 Å.

Ключові слова: талій телуриди, фазові рівноваги, твердий розчин, рентгенофазовий аналіз, диференційно-термічний аналіз, скануюча електронна мікроскопія.